





The effect of the stern wedge length and height on the drag and trim of a chine-planing hull

Mohammad A. Ghassemi¹, Parviz Ghadimi², Sayyed Mahdi Sajedi³

¹  <https://orcid.org/0000-0002-7412-7384>

²  <https://orcid.org/0000-0002-9315-5428>

³  <https://orcid.org/0000-0002-6421-5030>

Amirkabir University of Technology
424 Hafez Ave, Tehran, Iran,
e-mail: ¹marefghassemi@gmail.com, ²pghadimi@aut.ac.ir, ³sajfar1669@aut.ac.ir
 corresponding author

Keywords: chine-planing hull, stern wedge, wedge width and height, drag, trim, pressure distribution

JEL Classification: C61, C63, C65, L95

Abstract

This paper examines the effect of the stern wedge length and height on the drag and trim of a chine-planing hull in calm water. To this end, fluid flow was simulated by Star-CCM+ software by applying an overset mesh and $k-\varepsilon$ turbulent model. The finite volume method was used to discretize the fluid domain, and the fluid volume was utilized to capture the generated free surface. The considered model is a prismatic planing hull with a deadrise angle of 24° , a mass of 86 kg, a length (L) of 2.64 m, and a beam (B) of 0.55 m. For validation, the numerical results of drag and trim were compared against experimental data, which displayed good compliance. Subsequently, the hydrodynamic performance of the planing hull was investigated, and the wedge effect was assessed. The stern wedge was located at the bottom and near the aft perpendicular to the hull to facilitate a moderate distribution. Various wedge lengths of $0.2B$, $0.5B$, and B at two different heights of 5 mm and 10 mm were examined to assess the hydrodynamic performance of the hull at various speeds. The trim angle, resistance, water surface elevation, porpoising, roster tail, and the stern and bow were computed and analyzed. Based on the numerical results, it was concluded that when the wedge length increased, the drag and trim were reduced. It was also concluded that the best wedge for a vessel with desirable wake generation is one with a length of $0.2B$ and a height of 5 mm.

Introduction

Designers have attempted to reduce the drag of planing crafts to reduce their fuel consumption, environmental pollution, and provide more benefits to their owners. There are several devices to reduce the drag of these vehicles, including stern flaps, stern wedges, trim-tab, interceptors, air cavity injection, riblets, and boundary layer additives. The stern wedge is the focus of the current study. A stern wedge is a passive control system that changes the

hydrodynamic performance of a planing hull. It is located at the stern of the ship to provide a moderate pressure distribution. The length and height of the stern wedge may affect the drag, lift, and trim.

Experimental and numerical results of three types of appendages on the forward drag reduction of displacement and semi-displacement hulls were presented by Salas and Tampier (Salas & Tampier, 2013). They obtained a reduction in forward drag in all three tested devices (5–10%), showing potential fuel savings by evaluating the hydrodynamic effects

of energy-saving appendages. Millward (Millward, 1976) investigated the effect of stern wedges or trim tabs on two models of DTMB Series 62 planing hulls. The results confirmed that a stern wedge has an important effect on the dynamic lift of the hull, and he concluded that there is a change in drag other than that resulting from controlling the trim angle. A computer program (Jensen & Latorre, 1992) was used to calculate stern wedges and trim tabs to examine their influence on the drag of a motor yacht and powerboat. The US Navy (Karafiath, Cusanelli & Lin, 1999) employed stern wedges and stern flaps for DDG51 destroyers. They found a ~6% reduction in powering at top speed by model tests and computational fluid dynamics (CFD) analysis. Practical design characteristics of some appendages like side thrusters, shaft struts, and stern wedges were employed on passenger ships, and CFD analyses and model tests were conducted at Samsung Company (Jang et al., 2009). A flap was mounted at the stern of a barge operated by a pusher tug (Amacher et al., 2015), and the optimum flap shape was determined from numerical and physical modeling. The effect of a stern flap on the drag performance of the planing hull crew boat was presented by model tests (Yaakob, Shamsuddin & Koh, 2004). Five different stern flap designs were tested as part of a systematic investigation to determine the optimum geometrical characteristics of the stern flap. A preliminary study of a new stern device to improve efficiency in a fishing vessel was carried out by Pelaez et al. (Peláez et al., 2010). The drag and seakeeping characteristics of fast transom stern hulls were predicted by strip theory and model tests (Lahtiharju et al., 1991). A hydrodynamic design process was carried out for an optimum stern flap appendage to HALIFAX Class frigates (Cumming et al., 2006). This research showed that a suitable stern appendage reduced the fuel costs from 5% to 10%, depending on the operational profile of the ship. The effects of a stern wedge on the performance of planing craft in calm water were experimentally investigated for three different stern wedge types (Ghadimi, Sajedi & Tavakoli, 2019). They extended their study to the statistical analysis of the stern wedge effect on the seakeeping of a planing hull in irregular waves at the onset of the planing region (Ghadimi, Sajedi & Taghikhani, 2018). The effect of a stern wedge on the powering performance and annual fuel consumption of destroyer and frigate-sized ships was investigated by (Karafiath & Fisher, 1978). The effects of various stern wedge configurations on the calm water performance of this model were experimentally systematically investigated for volumetric

Froude numbers up to 3.0 (Grigoropoulos & Loukakis, 1996).

The RANS equations with standard k -turbulent model coupled with a VOF multiphase model were solved in a specifically generated mesh for turbulent free-surface flow (Ghassemi, Kamarlouei & Veysi, 2015; Veysi et al., 2015). A hydrodynamic investigation into the Naples Systematic Series model was also conducted. An extended verification and validation study using CFD simulations was carried out for planing Hulls (De Luca et al., 2016). Recently, comprehensive experimental and numerical works on various types of stern wedges of planing hulls were carried out by Ghadimi et al. (Ghadimi, Sajedi & Taghikhani, 2018; Izadi et al., 2018). In these studies, they investigated how installing a wedge and changing its height affected the hydrodynamic performance of the craft. They concluded that installing a wedge improved the craft's stability, reduced the trim angle, and increased the CG and resistance.

Based on the reviewed literature, various attempts have been made to analyze different aspects of appendages for longitudinal stability; however, no parametric study has been performed on the shape or length of the wedge and its effects on the resistance and trim of a vessel. In this article, the effect of wedge length on the resistance, trim, and pressure contours of a vessel in calm water was investigated. Accordingly, a two-phase flow was simulated by Star-CCM+ software applying an overset mesh and k -turbulent model. The finite volume method was used to discretize the fluid domain and fluid volume to capture the generated free surface. The results associated with resistance and trim were compared against experimental data for validation purposes. Subsequently, different wedge lengths were examined at different Froude numbers, and resistance, trim, pressure contours, and water surface elevations were computed and analyzed.

Problem statement

In this current paper, the hydrodynamics of a planing monohull and a hard-chine vessel with a V-shaped body is considered. The boat is supposed to reach a planing speed that is characterized by a Froude Number. Froude Numbers less than 0.4 are considered to be in the displacement regime, while Froude Numbers between 0.4 and 1.0 are considered to represent the semi-planing condition. On the other hand, Froude Numbers beyond 1.0 are recognized as the planing regime. At each speed, it is expected that the boat will reach a dynamic equilibrium. If the

forces cannot reach a dynamic equilibrium, a trim angle and CG will increase, and the boat will reach a non-equilibrium condition in which it exhibits the porpoising phenomenon. In this situation, the use of wedges as appendages can help the vessel overcome this instability.

Geometry

Ghadimi et al. (Ghadimi, Sajedi & Tavakoli, 2019) performed various experimental tests at the Persian Gulf National Laboratory on two planing hull models: one with a wedge and the other without a wedge. The specifications are listed in Table 1. The results of these experiments (Ghadimi, Sajedi & Tavakoli, 2019) were used to validate the current numerical results. The selected model is a chine-planing hull. The main dimensions of the model are given in Table 1. The body plan is shown in Figure 1. The length of the model was 2.4 m and the mean deadrise angle was 24°.

Table 1. Main dimensions of the model

Parameter	Value
Length (L) (m)	2.4
Breadth (B) (m)	0.55
Draft (T) (m)	0.146
Deadrise angle (deg)	24
VCG (m)	0.184
LCG from transom (m)	0.791
Mass (M) (kg)	86.024
Stern wedge length	(0.2) B

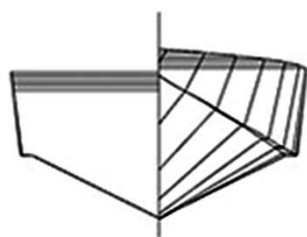


Figure 1. The body plan of the model

The experimental results are shown in Tables 2 and 3 for the examined models. As observed in Table 2, the model without a wedge displayed longitudinal instability at 8 m/s.

The parent model has no wedge and thus, different lengths of the stern wedge, i.e., $0B$ (without a stern wedge), $0.2B$, $0.5B$, and $1B$ (where B is the breadth of the hull) were considered; therefore, four models were examined: one without a stern wedge and three with different stern wedge models. Figure 2

Table 2. Measured values for the case without a wedge (Ghadimi, Sajedi & Tavakoli, 2019)

V (m/s)	τ_s (deg)	Z_{CG} (mm)	τ (deg)	R_T (KgF)
1	2.34	-1.78	2.47	0.8
2	2.34	-8.67	3.73	5.4
3	2.34	4.03	6.17	11.55
4	2.34	26.71	6.77	13.05
5	2.34	52.61	7.39	13.94
6	2.34	70.26	6.63	13.65
7	2.34	81.54	5.81	13.8
8	2.34	PORP.	PORP.	PORP.

Table 3. Measured values for the case with a wedge 0.2B (Ghadimi, Sajedi & Tavakoli, 2019)

V (m/s)	τ_s (deg)	Z_{CG} (mm)	τ (deg)	R_T (KgF)
1	2.34	-0.71	2.36	1.028
2	2.34	-5.37	3.24	5.75
3	2.34	8.07	4.93	10.5
4	2.34	27.28	4.35	11.00
5	2.34	42.42	3.77	11.79
6	2.34	54.65	2.96	12.75
7	2.34	62.84	2.01	14.56
8	2.34	63.18	1.16	17.7

displays the stern wedge at the bottom of the hull. The height of the considered wedge in all models was 10 mm.

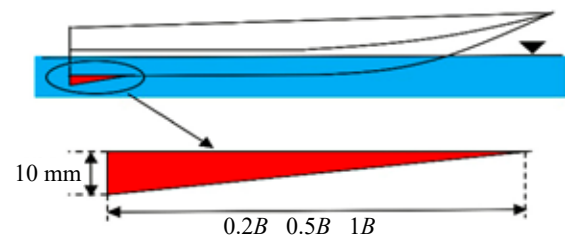


Figure 2. Stern wedge on the hull

Numerical study

All experiments were numerically simulated using the Star-CCM+ software, which is based on the finite volume method (FVM). To this end, the unstable dynamics of the mono-hull high-speed craft were investigated to determine the resistance of the craft, as well as the heave and pitch motions by mounting different wedges. It should be noted that these wedges are mounted at the center of gravity, and the vessel was assumed to exhibit 2° of freedom in three-dimensional space.

Governing equations

The governing equations of the turbulent incompressible flow include the continuity and Navier-Stokes equations. By applying Reynolds averaging, the RANS equations were obtained as

$$\frac{\partial}{\partial x_i}(\bar{u}_i) = 0 \quad (1)$$

$$\begin{aligned} \frac{\partial}{\partial x_j}(\rho \overline{u_j u_i}) &= -\frac{\partial \bar{P}}{\partial x_i} + \\ &+ \frac{\partial}{\partial x_j} \left[\mu \left(\frac{\partial \bar{u}_i}{\partial x_j} + \frac{\partial \bar{u}_j}{\partial x_i} - \frac{2}{3} \delta_{ij} \frac{\partial \bar{u}_i}{\partial x_i} \right) \right] + \frac{\partial}{\partial x_j}(\rho \overline{u'_j u'_i}) \end{aligned} \quad (2)$$

Here \bar{u}_i and \bar{u}_j are the time mean of the velocity component, ($i, j = 1, 2, 3$), \bar{p} is piezometric pressure coefficient, ρ is fluid density, μ is coefficient of dynamic viscosity, $\rho \overline{u'_j u'_i}$ is the Reynolds stress term.

The most commonly used turbulence models are two-equation models whose function is to form a relationship between the turbulence viscosity with longitudinal scales and turbulence velocities. In these models, there seems to be a good equilibrium between computational costs and the accuracy of the results.

All two-equation turbulence models used the turbulence kinetic energy (k) as the first variable, while the second transfer equation was written for an unknown variable. The turbulence models differed from each other. One of the standard turbulence models used in the industry is the k - ε model, which offers good precision and stability. This turbulence model is divided into three sub-models including standard k - ε , realisable k - ε , and RNG k - ε . The realisable k - ε turbulence model is used in this study. The modeled transport equations for k and ε for steady-state and incompressible flow are given by

$$\frac{\partial}{\partial x_i}(\rho k \bar{u}_i) = \frac{\partial}{\partial x_j} \left[\left(\mu + \frac{\mu_t}{\sigma_k} \right) \frac{\partial \varepsilon}{\partial x_j} \right] + G_k - Y_k \quad (3)$$

$$\frac{\partial}{\partial x_i}(\rho \varepsilon \bar{u}_i) = \frac{\partial}{\partial x_j} \left[\left(\mu + \frac{\mu_t}{\sigma_\varepsilon} \right) \frac{\partial \varepsilon}{\partial x_j} \right] + G_\varepsilon - Y_\varepsilon \quad (4)$$

In Equations (3) and (4), σ_k and σ_ε are the turbulent Prandtl numbers for k and ε , respectively. μ_t is the turbulent viscosity, and k is the turbulent kinetic energy. The production of turbulence kinetic energy,

G_k is approximated in a manner consistent with the Boussinesq hypothesis as:

$$G_k = \mu_t S^2 \quad (5)$$

where S is the modulus of the mean rate-of-strain tensor, defined by

$$S = \sqrt{2S_{ij}S_{ij}} \cdot S_{ij} = \frac{1}{2} \left(\frac{\partial \bar{u}_j}{\partial x_i} + \frac{\partial \bar{u}_i}{\partial x_j} \right) \quad (6)$$

The dissipation of this turbulence kinetic energy, Y_k , is defined by

$$Y_k = \rho \varepsilon \quad (7)$$

The production and diffusion terms in the transport equation for ε differ slightly and are defined as

$$G_\varepsilon = \rho C_1 S \varepsilon, \quad Y_\varepsilon = \rho C_2 \frac{\varepsilon^2}{k + \sqrt{\nu \varepsilon}} \quad (8)$$

where C_2 is a constant, and C_1 is defined as

$$C_1 = \max \left[0.43 \cdot \frac{\eta}{\eta + 5} \right], \quad \eta = S \frac{k}{\varepsilon} \quad (9)$$

The turbulent viscosity is computed through a formulation of k and ε , given as

$$\mu_t = \rho C_\mu \frac{k^2}{\varepsilon} \quad (10)$$

where C_μ is calculated using the following equation:

$$C_\mu = \frac{1}{A_0 + A_s \frac{kU^*}{\varepsilon}} \quad (11)$$

where

$$U^* = \sqrt{S_{ij}S_{ij} + \tilde{\Omega}_{ij}\tilde{\Omega}_{ij}} \quad (12)$$

$$\tilde{\Omega}_{ij} = \frac{1}{2} \left(\frac{\partial \bar{u}_i}{\partial x_j} - \frac{\partial \bar{u}_j}{\partial x_i} \right) \quad (13)$$

A_0 is a constant and the remaining variable, A_s , is calculated using the following relation:

$$A_s = \sqrt{6} \cos \phi \quad (14)$$

where:

$$\phi = \frac{1}{3} \cos^{-1}(\sqrt{6}W), \quad W = \frac{S_{ij}S_{jk}S_{ki}}{\tilde{S}^3} \quad (15)$$

where $\tilde{S} = \sqrt{S_{ij}S_{ij}}$ and the constants applied in the realisable k - ε turbulence model are set to be

$$\sigma_k = 1.0, \sigma_\varepsilon = 1.2, C_2 = 1.9, \text{ and } A_0 = 4.04.$$

Computational domain

The computational domain is illustrated in Figure 3.

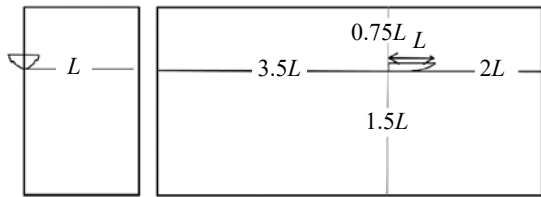


Figure 3. Computational domain

The water depth was considered to be 1.5 times the vessel length, and the free surface from the top of the domain was assumed to be 0.75 times the length of the vessel.

Boundary conditions

As shown in Figure 4, the required boundary conditions are applied as follows:

- 1) The boundary conditions for the front and top faces of the computational domain are prescribed as uniform velocity.
- 2) A symmetric boundary condition was applied on the left side face.
- 3) The craft model and bottom were simulated as a wall in a no-slip condition.
- 4) On the back face, the pressure condition was applied as the boundary condition.

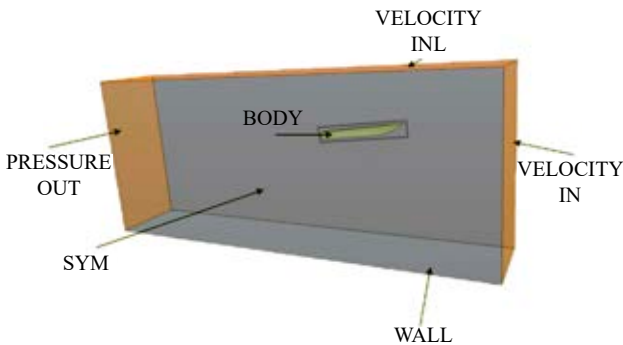


Figure 4. Computational domain and applied boundary conditions

The free surface models

A comparison of the different free-surface simulation techniques available in the existing CFD codes is described in the report of Gothenburg 2010 workshop (ITTC, 2011), which is shown in Figure 5. The volume of fluid (VOF) method is the most popular choice, followed by the level-set method (5 codes, 17%). Only three of the 33 existing codes (9%) use free-surface fitting methods.

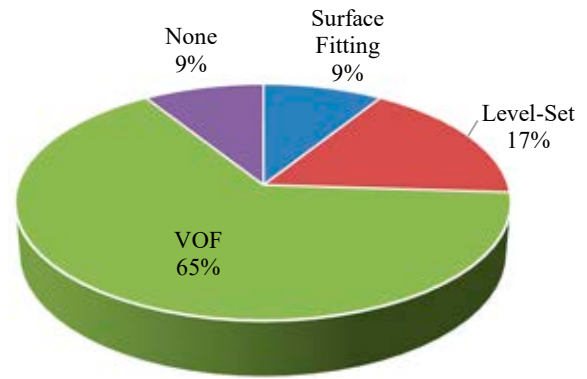


Figure 5. Gothenburg Workshop 2010 – free surface models in the widely used CFD codes (Scognamiglio, 2017)

The VOF method is widely used as a free-surface scheme that is implemented by Star CCM+. The VOF method employs the concept of an equivalent fluid. This approach assumes that the (two) fluid phases share the same velocity and pressure fields, thereby allowing them to be solved with the same set of governing equations describing momentum and mass transport as in a single-phase flow.

Dynamic meshing and mesh generation

In order to capture motion, the mesh structure must change dynamically with the moving object. There are different methods for the dynamic movement of the mesh. The three most suitable for hull simulations are the simple moving grid, the diffusion-based smoothing method/morphing grid, and the Overset/Chimera grid. The “overset method” is hereby used to create the moving mesh, and the method is illustrated in Figure 6.

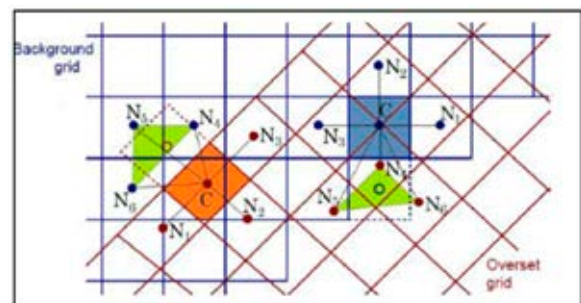


Figure 6. Mix overset and Tank Mesh (Scognamiglio, 2017)

Two areas are involved in the overset method: one for the moving part and another for the fixed part. The moving part, known as an overset, uses the displacement method of the network to move the object. The generated mesh grid is shown in Figure 7.

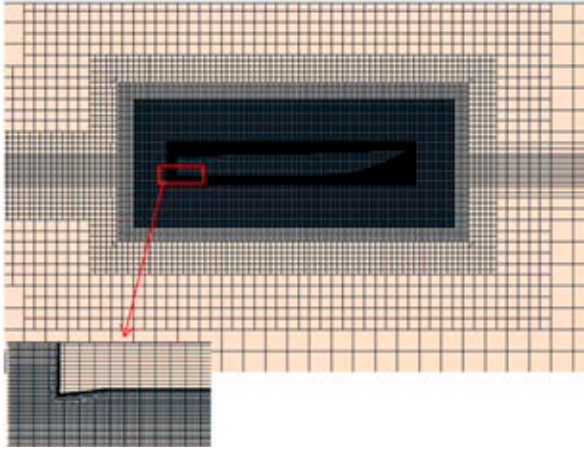


Figure 7. Meshing on the whole domain and stern wedge

The y^+ value at each point of the craft is shown in Figure 8. At the studied speeds, the resulting y^+ was found below 100; therefore, it can be claimed that different areas are covered by the turbulent flow boundary layer.

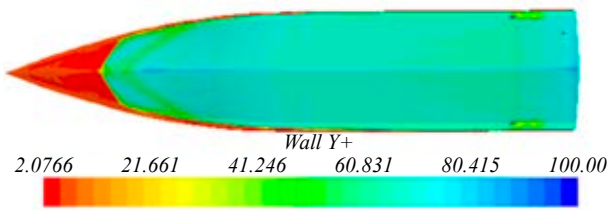


Figure 8. Values of y^+ at different points of the craft, equipped with a 10 mm wedge, at a speed of 7 m/s. Based on the ITTC recommendation, when the wall function was used, the y^+ can be increased to 300

Mesh independency study

To study the effect of mesh size on the hydrodynamic parameters, a coarse mesh, a medium mesh,

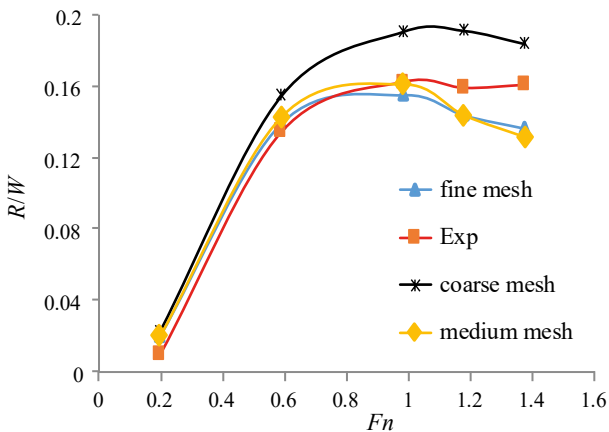


Figure 9. Comparison of resistance/weight (R/W) ratios for three meshes by experimental data (without a stern wedge)

and a fine mesh are considered. The number of the coarse mesh is about $1.5 \cdot 10^6$, the number of the medium mesh is $3 \cdot 10^6$, and the number of the fine mesh is $7 \cdot 10^6$. The results of the resistance parameters used for validation are displayed in Figure 9.

As evident in Figure 9, the results of medium and fine meshes related to the resistance are in good agreement with the experimental results; therefore, a medium mesh was adopted for the computational efficiency.

Validation

The resistance, trim, and pressure distribution, as well as water surface level were computed for the vessels with or without a wedge. The computations were performed at different speeds and for different lengths and heights of the wedge.

Validation of the results related to the vessel with no wedge

In this section, validation of the results pertinent to the vessel with no wedge are presented. The plots of resistance/weight (R/W) ratio, as well as trim angle versus Froude number are displayed in Figures 10 and 11, respectively.

As evident in Figure 10, although there is some discrepancy between the numerical and experimental data at high Froude numbers Fn , the results generally follow a similar trend. As observed in Figure 10, the peak of the R/W plot occurs at $Fn = 0.7$ for a vessel with no wedge, and then the resistance decreases. The RMS value was computed to be 0.01323.

In Figure 11, where the craft has no wedge, the trim versus Fn is plotted for both experimental and

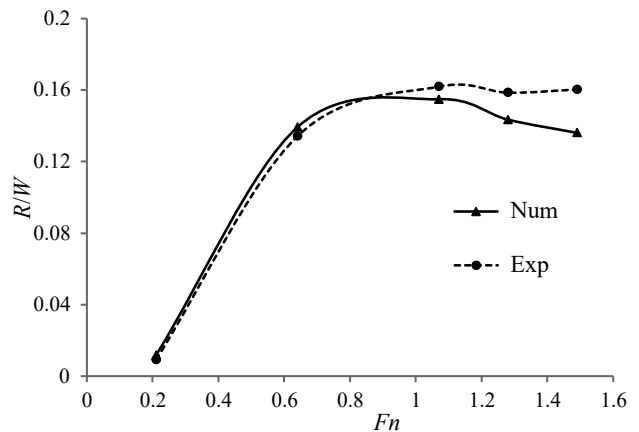


Figure 10. Comparison of R/W vs. Fn (for the vessel without a stern wedge)

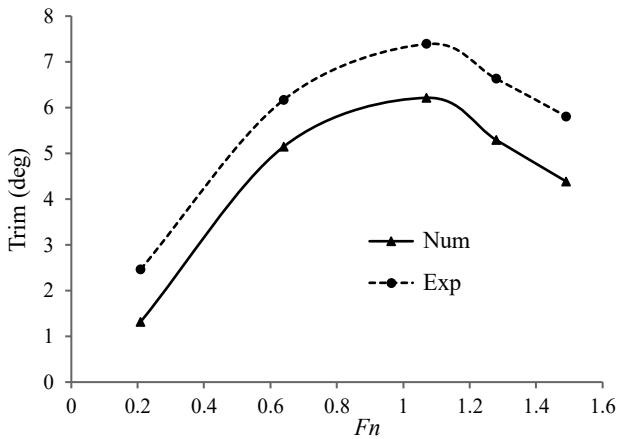


Figure 11. Comparison of trim vs. F_n (for the vessel without a stern wedge)

numerical modeling results. In this figure, the trim increases upon increasing F_n to nearly 1, followed by a decrease in both curves.

The computed wave and pressure contours for these cases will be discussed in Section *Influence of length*.

Validation in the case of a vessel with a wedge with a length of 92 mm and a height of 10 mm

Figures 12 and 13 were also used for validation. Figure 12 shows the ratio of resistance to weight versus F_n , while Figure 13 displays the plot of trim versus F_n . These results correspond to a vessel equipped with a wedge with a length of 92 mm and a height of 10 mm.

The numerical results displayed in both graphs are very similar to the experimental results. The RMS in Figure 12 was calculated to be 0.0089. As shown in Figure 12, when a wedge was used, the peak occurred at $F_n = 0.65$. The important conclusion drawn from the presented results is the fact that the stern wedge causes the vessel to

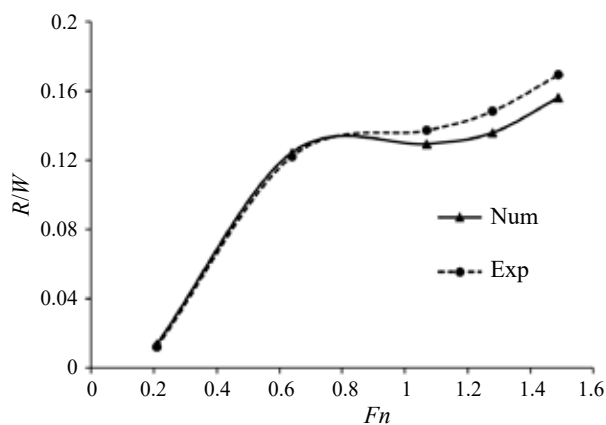


Figure 12. Comparison of result R/W vs. F_n for stern wedge length = $0.2B$ and height = 10 mm

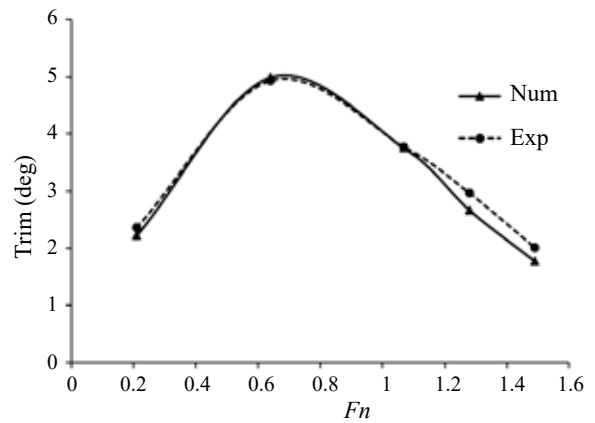


Figure 13. Comparison of result trim vs. F_n for stern wedge length = $0.2B$ and height = 10 mm

reach the planing regime more quickly. Afterwards, upon increasing the Froude number, the resistance increases.

When the craft has a 92 mm length wedge, the trim increases upon increasing the Froude number to nearly 0.6 and subsequently decreases in both experimental and numerical curves.

Validation of a vessel with a wedge with a 92 mm length and 5 mm height

Figure 14 shows the non-dimensional resistance to weight ratio versus F_n , while Figure 15 presents the trim versus F_n . The studied vessel has a wedge with a length of 92 mm and a height of 5 mm.

As shown in Figure 14, the resistance increased up to $F_n = 0.7$ and then decreased. The resistance variation is very similar to the non-wedge state in Figure 10. The RMS in R/W vs. F_n was determined to be 0.01142, and a comparison of the numerical and experimental results shows good agreement.

Figure 15 illustrates changes in trim versus F_n , which shows that the R/W ratio also increases up

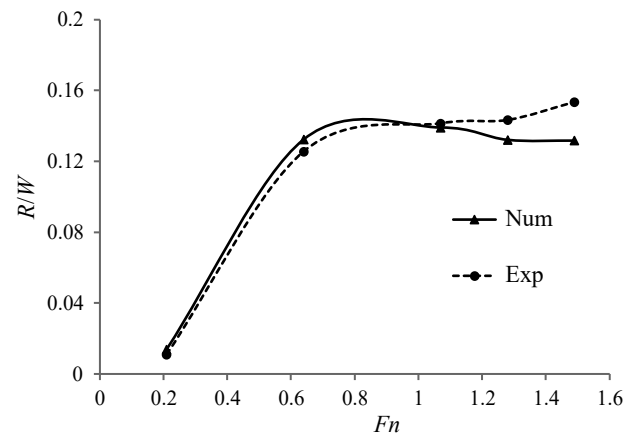


Figure 14. Comparison of result R/W vs. F_n for stern wedge length = $0.2B$ and height = 5 mm

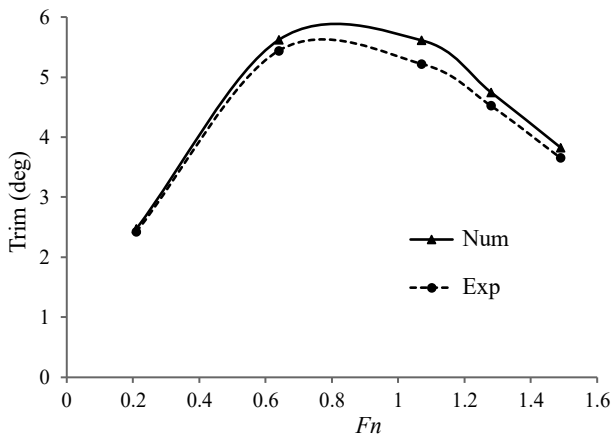


Figure 15. Comparison of result trim vs. Fn for stern wedge length = $0.2B$ and height = 5 mm

to $Fn = 0.7$ and then decreases. As expected, the numerical findings are in good compliance with the experimental curve, and there is a relatively small error.

Results and discussion

The resistance, trim, and pressure distribution, as well as the water surface level, were computed for vessels with or without a wedge. The computations were performed at different speeds and for wedges with different lengths and heights.

Influence of length

A comparison of the R/W versus Fn for various stern wedge lengths is demonstrated in Figure 16. In this section, modeling was carried out at two lengths of $0.5B$ and $1B$. This modeling was used to determine the wedge's longitudinal effects on the craft's performance. The chart of resistance versus Froude

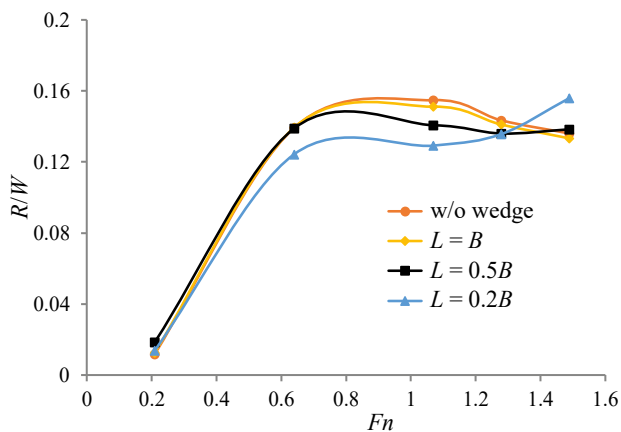


Figure 16. Comparison of the R/W vs. Fn for various stern wedge lengths with a height of 10 mm

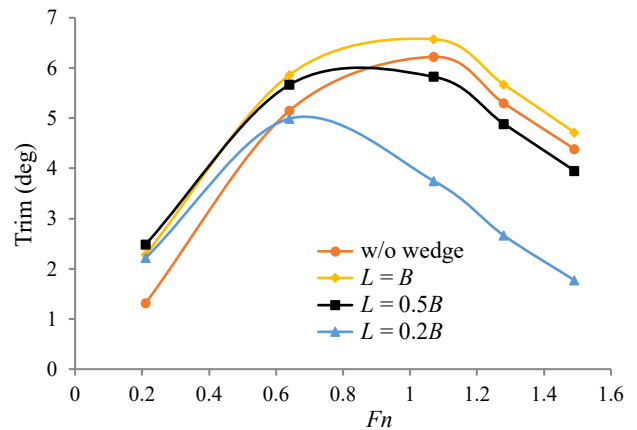


Figure 17. Comparison of the trim vs. Fn for various stern wedge lengths with a height of 10 mm

numbers is given in Figure 16 for four models – without a wedge and wedges with lengths of $0.2B$, $0.5B$, and $1B$. The trim distribution versus Fn for these lengths is also presented in Figure 17.

As shown in Figure 16, in the starting area of the planing (about $Fn = 0.9$), the minimum resistance corresponds to a wedged model with $0.2B$ length, and the maximum resistance was obtained for the non-wedged model. The lift at the stern of the high-speed craft increases due to the placement of the wedge. As the stern lift increases, the stern draft surface decreases, as well as the craft's resistance; however, the craft's resistance increases at $Fn = 1$ due to an increase in the wet surface of the craft's bow. By increasing the wedge length, its effect decreases in the planing area. In general, the best operating conditions in the planing area and beyond were obtained at a length of $0.5B$.

The plot of trim versus Froude numbers in Figure 17 shows that trim decreases as the wedge length decreases. Reducing the ratio of length to height in the wedge increases the hydrodynamic pressure on the stern. By increasing the stern pressure, the lift in the transom region increases, and the craft's bow dips into the water. The maximum bow trim is related to the craft without a wedge. In this case, the craft is unstable. The craft becomes stable for all lengths by adding a wedge at the stern.

Effect of height

In this section, the effect of height was investigated by considering a wedge with a 5 mm height. Again, plots of resistance to weight ratio versus Froude number for different lengths are displayed in Figure 18, and plots of trim versus Fn are shown in Figure 19. It should be noted that the height

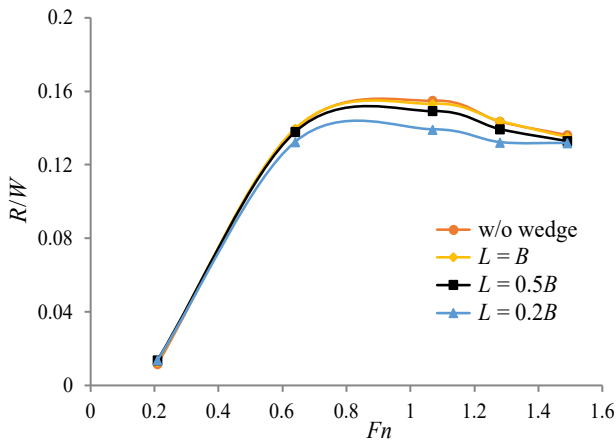


Figure 18. Comparison of the R/W vs. Fn for various stern wedge lengths with a height of 5 mm

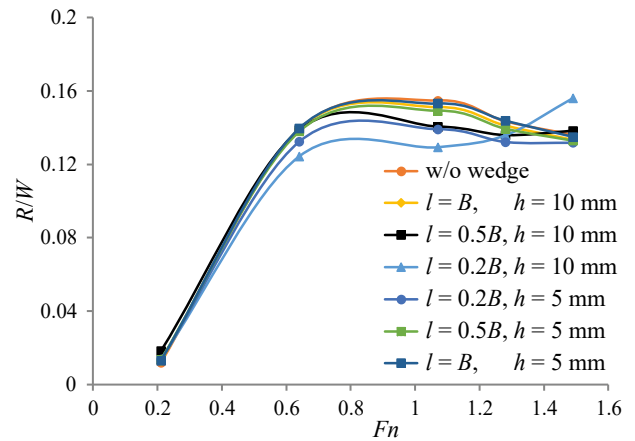


Figure 20. Comparison of the R/W vs. Fn for various stern wedge lengths and heights

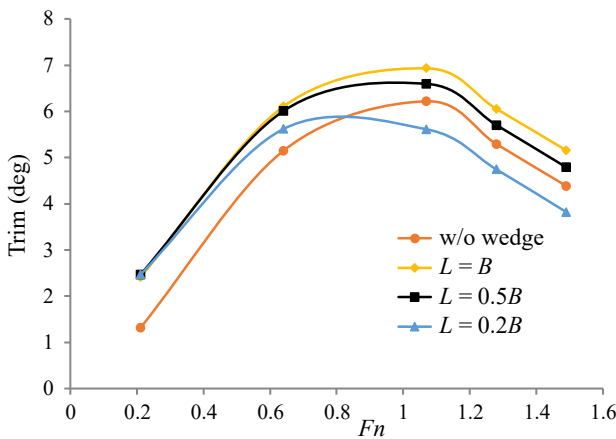


Figure 19. Comparison of the trim vs. Fn for various stern wedge lengths with a height of 5 mm

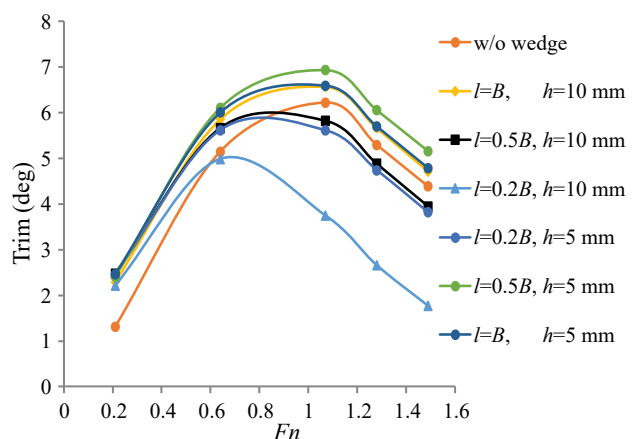


Figure 21. Comparison of trim vs. Fn for various stern wedge lengths and heights

considered here is half the size of the height studied in the section *Influence of length*.

In Figure 18, similar to the results in the previous section, upon increasing wedge length, the resistance decreased for all wedges. Meanwhile, the maximum reduction was related to the wedge with a 5 mm height and $0.2B$ length. Figure 19 that displays the trim versus Froude number. When a wedge was used, the trim increased, except for one case. In the vessel with a wedge with a $0.2B$ length and height of 5 mm, the trim decreased above a Froude number of approximately 0.7.

Simultaneous effect of height and length

In this section, plots of section *Influence of length* and *Effect of height* are combined and superposed in one figure to better understand the simultaneous effect of height and length of the wedge. Accordingly, Figures 20 and 21 show eight models of

crafts, including different geometries of wedges and non-wedge.

Figure 20 demonstrates that when a wedge with a length $0.2B$ and height 10 mm is used, the resistance increases at $Fn = 1.6$ due to an increase in wedge height. The exerted pressure on the bottom increases, and as a result, the trim decreases, and the resistance increases.

Figure 21 also displays a plot of trim versus Froude numbers for seven models of non-wedged and wedged crafts with lengths of $0.2B$, $0.5B$, and $1B$ with heights of 10 mm and 5 mm. As observed in this figure, the trim decreases upon decreasing the wedge length. Reducing the ratio of length to height in the wedge increases the hydrodynamic pressure on the stern. By increasing the stern pressure, the lift in the transom region increases, and the craft's bow dips into the water. Most bow trim was related to the craft without a wedge except at $Fn = 1.5$. In this case, the craft is unstable. The craft becomes stable

for all lengths and heights by adding a wedge at the stern.

In general, the best operating conditions in the planing area and beyond were obtained at a length of $0.2B$ and a height of 5 mm.

Analysis of porpoising

One of the most important problems in high-speed craft is the porpoising phenomenon, which involves heaving and pitch motions. Figure 22 shows trim against time for the vessel without a wedge, while Figure 23 shows trim against time for the vessel with a wedge.

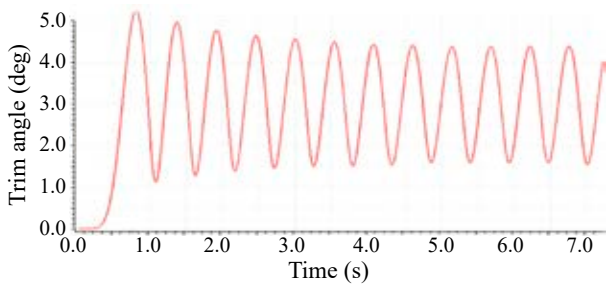


Figure 22. Trim versus time for a vessel without a wedge

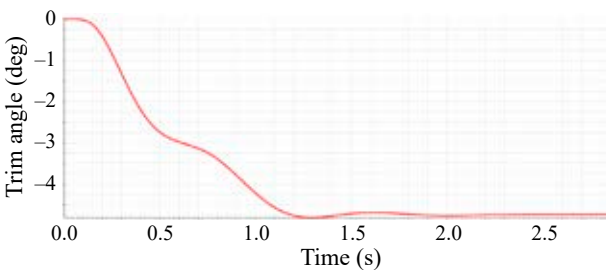


Figure 23. Trim versus time for a vessel with a wedge

As shown in Figure 22, the vessel without a wedge is not stable and permanently vibrates; however, when a wedge was mounted on the vessel,

the porpoising phenomenon was eliminated. This is indeed the most positive aspect of using a wedge. Figure 23 demonstrates that vibration was damped after 2 seconds in a vessel with a wedge.

Wave and pressure contours

The wave and pressure contours are displayed in Figure 24 for a non-wedged vessel and a vessel with a wedge length of $0.2B$.

As evident in Figure 24, by increasing the speed, the transverse wavelength increases but becomes narrower. The reason for the narrowing of the transverse waves is a reduction in the stern draft; therefore, by adding a wedge at the stern of the high-speed craft, the transverse waves become wider.

Figure 25 shows the pressure contours of non-wedged and wedged crafts with different lengths and heights of 5 mm and 10 mm at a speed of 5 m/s.

As shown in Figure 25, the first row has wedges with different lengths and an identical height of 5 mm, which moves the center of pressure to the front by increasing the length wedge. Also, a V-shaped pressure distribution is apparent in front of the vessel upon increasing the wedge length.

The second row of Figure 25 corresponds to vessels with a different wedge length but an identical height of 10 mm. By increasing the wedge length, the pressure distribution was greater in a particular region and less dispersed than in previous cases. The V shape observed on the vessel front was related to a pressure increase in this area, which also existed in the previous row. It is interesting to know that, like the preceding row, the center of buoyancy was moved forward and by increasing the wedge length, and the maximum pressure that enters the center of the buoyancy decreased; therefore, the maximum pressure in this row belongs to plot (d), which tolerated a maximum compression of 3291.4 Pa.

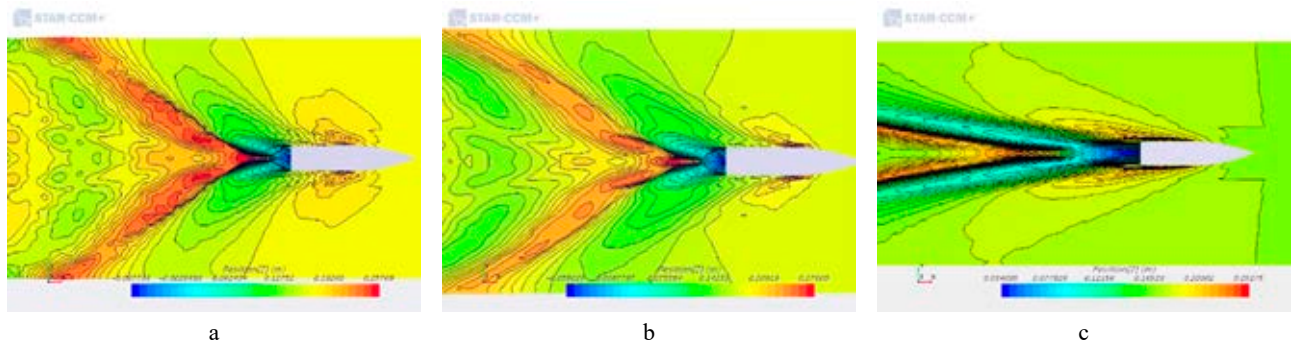


Figure 24. Wave contour of two models at two speeds: a) no stern wedge, $Fn = 0.5895$, b) with a stern wedge ($l = 0.2B$), $Fn = 0.5895$, and c) with a stern wedge ($l = 0.2B$), $Fn = 0.5895$

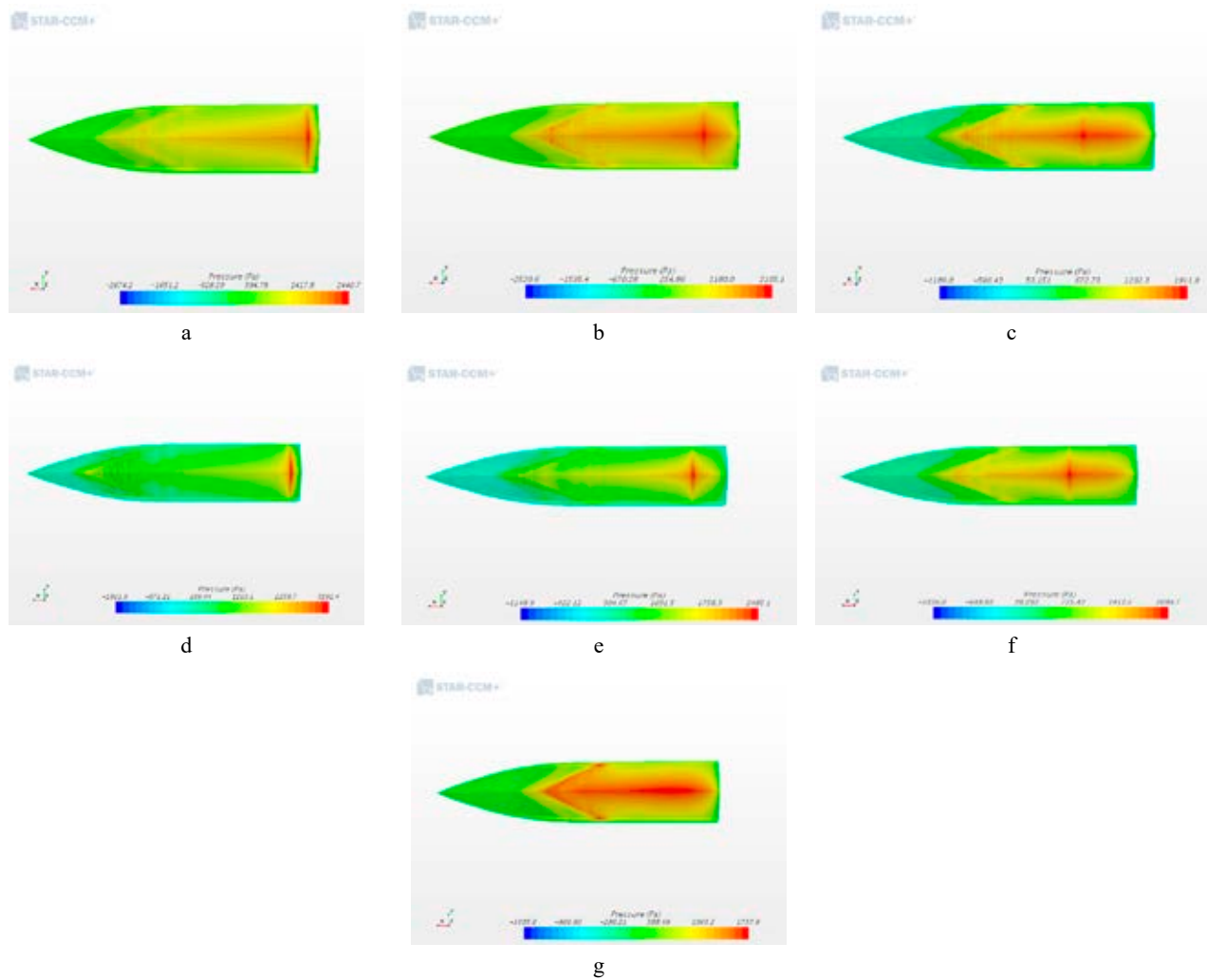


Figure 25. Pressure distribution contour of two models at two speeds: a) with a stern wedge ($l = 0.2B, h = 5$ mm), b) with a stern wedge ($l = 0.5B, h = 5$ mm), c) with a stern wedge ($l = B, h = 5$ mm), d) with a stern wedge ($l = 0.2B, h = 10$ mm), e) with a stern wedge ($l = 0.5B, h = 10$ mm), f) with a stern wedge ($l = B, h = 10$ mm), g) no stern wedge; all of them $Fn = 0.9825$

Plot (g) presents the pressure distribution of a vessel with no wedge. As observed, the pressure was distributed along the length and width of the vessel in a V-shaped plot. As described in previous figures, this is not desirable. The maximum pressure in this case was found to be 1737.9 Pa. As shown in Figure 25, placing a wedge on the stern of the craft caused a pressure generation in a region, which improved the dynamic stability.

Generated wake behind the vessel

High-speed crafts are categorized in two ways. The first method is by craft noise, while the second method is by water spray. In this paper, the water spray generated behind the propeller in the form of a rooster tail is examined. Figure 26 shows the water spray generated behind the craft without a wedge and those with wedges with different lengths and heights at different velocities.

Figure 26 illustrates the wake generated behind the vessel. The first three rows of the plots are related to vessels with wedges with different lengths and a height of 5 mm. In these plots, when the length of the wedge increases from 92 mm to 275 mm, the height of the generated wave behind the vessel also increases. As observed, the wave height decreases when the length of the wedge increases. The second three plots in Figure 26 are related to vessels with wedges with different lengths and a height of 10 mm. In this row, by increasing the length of the wedge, the average height of the water behind the vessel increases. The wave height in (e) and (f) is such that, at low velocity, the height is low, and then it increases and eventually decreases again. The last plot is related to a vessel without a wedge. The behavior of the wake behind this vessel is very similar to that of Figure 25 and the height of water behind the high-speed craft is approximately equal to the height in plot (g). From the results presented in Figure 26, one

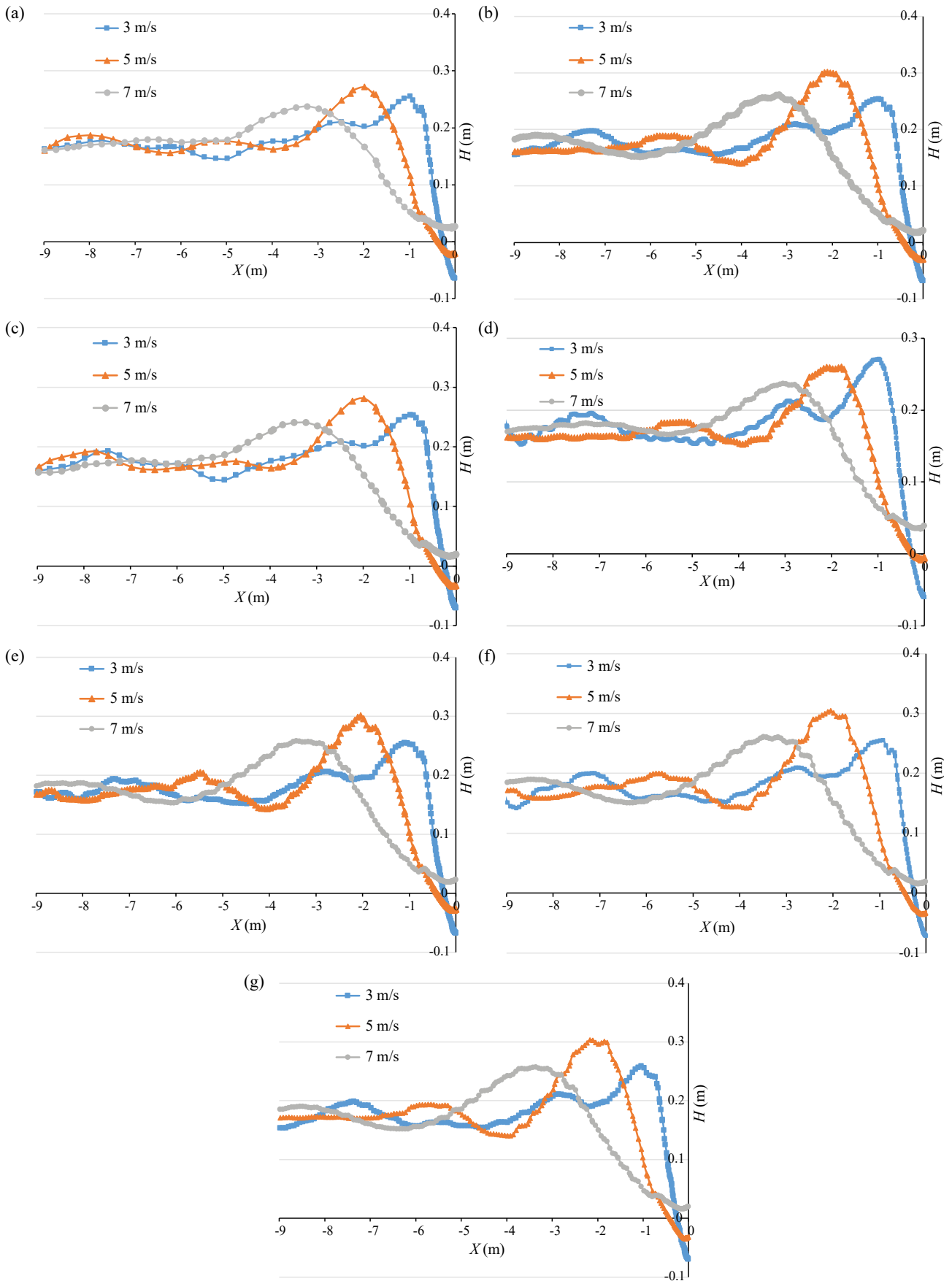


Figure 26. Generated wake behind the vessel with a) stern wedge ($l = 0.2B$, $h = 5$ mm), b) stern wedge ($l = 0.5B$, $h = 5$ mm), c) stern wedge ($l = B$, $h = 5$ mm), d) stern wedge ($l = 0.2B$, $h = 10$ mm), e) stern wedge ($l = 0.5B$, $h = 10$ mm), f) stern wedge ($l = B$, $h = 10$ mm), and g) without a stern wedge

may conclude that considering the wake behind the vessel, the best wedge for this vessel is the wedge in plot (g), in which the average height is lower than other models.

Conclusions

This paper examined the effect of stern wedge length on the trim and drag of a chine-planing hull in calm water. To this end, the fluid flow was simulated by Star-CCM+ software by applying an overset mesh and $k-\varepsilon$ turbulent model. The finite volume method was used to discretize the fluid domain, and the fluid volume was used to capture the generated free surface. The considered model was a prismatic planing hull with a deadrise angle of 24° , a mass of 86 kg, a length (L) of 2.64 m, and a beam (B) of 0.55 m. For validation purposes, the numerical results of the drag and trim were compared against experimental data, which displayed good compliance. Subsequently, the hydrodynamic performance of the planing hull was investigated, and the wedge effect was assessed. The stern wedge was located at the bottom and near the aft perpendicular to the hull to facilitate a moderate distribution. Various wedge lengths ($0.2B$, $0.5B$, and B) at two different heights were examined to assess the hydrodynamic performance of the hull at various speeds. The trim angle, resistance, rise-up at CG, water surface elevation, and stern and bow were computed and analyzed. Based on the numerical results, it was concluded that when the wedge length increases, the drag and trim decreased. The following are further conclusions drawn from the obtained results:

- For a stern wedge length of $0.2B$ and a height of 10 mm, less drag was produced, except at $Fn = 1.3755$, for which there was a small increase.
- When the stern wedge length increased, the drag also increased at both wedge heights of 5 and 10 mm.
- The stern wedge caused the vessel reach the planing zone, faster.
- Considering the drag, the best wedge was one with a length of $0.2B$ and a height of 5 mm.
- The lowest trim was the vessel with a length $0.2B$ and a height of 10 mm; however, in terms of resistance, the proper choice was a vessel with a wedge length of $0.2B$ and a height of 5 mm. In terms of trim, this is not a bad choice and ranks after the vessel with a $0.2B$ length and height of 10 mm.
- The most important aspect of wedge installation is the elimination of porpoising in high-speed craft. It is shown that installing a wedge in the

vessel focuses the pressure at a point and reduces porpoising. The maximum pressure at the bottom occurred for a vessel of $0.2B$ length and 10 mm height, but the best choice was a wedge with a length of $0.2B$ and a height of 5 mm.

- The rooster tail phenomenon was also investigated, and it was concluded that the best wedge for a vessel with desirable wake generation is one with a $0.2B$ length and a height of 5 mm.

Acknowledgment

This research received no specific grant from any funding agency in the public, commercial, or not-for-profit sectors, and there are no conflicts of interest.

References

1. AMACHER, R., LIECHTI, T.C., PFISTER, M., CESARE, G.D. & SCHLEISS, A.J. (2015) Wave-reducing stern flap on ship convoys to protect river banks. *Naval Engineers Journal* 127(1), pp. 95–102.
2. CUMMING, O., PALLARD, R., THORNHILL, E., HALLY, D. & DERVIN, M. (2006) *Hydrodynamic Design of a Stern Flap Appendage for the HALIFAX Class Frigates*. MARI-TECH 2006.
3. DE LUCA, F., MANCINI, S., SALVATORE, M. & PENZA, C. (2016) An extended verification and validation study of CFD simulations for planing Hulls. *Journal of Ship Research* 60(2), pp. 101–118, doi: 10.5957/JOSR.60.2.160010.
4. GHADIMI, P., SAJEDI, S.M. & TAGHIKHANI, P. (2018) Statistical analysis of wedge effect on the seakeeping of a planing hull in irregular waves at the onset of the planing region. *Journal of Applied Fluid Mechanics* 11(4), pp. 905–918.
5. GHADIMI, P., SAJEDI, S.M. & TAVAKOLI, S. (2019) Experimental Study of the Wedge Effects on the Performance of a Hard-chine Planing Craft in Calm Water. *Scientia Iranica B* 26(3), 1316–1334.
6. GHASSEMI, H., KAMARLOUEI, M. & VEYSI, S.T.G. (2015) A hydrodynamic methodology and CFD analysis for performance prediction of stepped planing hulls. *Polish Maritime Research* 2(86), 22, pp. 23–31.
7. GRIGOROPOULOS, G.J. & LOUKAKIS, T.A. (1996) *Effect of wedges on the calm water resistance of planing hulls*. 1st International Conference on Marine Industry, Varna, Bulgaria.
8. ITTC (2011) Recommended Procedures and Guidelines, 24th ITTC 7.5-03 02-02.1.
9. IZADI, M., GHADIMI, P., FADAVI, M. & TAVAKOLI, S. (2018) Hydroelastic analysis of water impact of flexible asymmetric wedge with an oblique speed. *Meccanica* 53(10), pp. 2585–2617.
10. JANG, H.S., LEE, H.J., JOO, Y.R., KIM, J.J. & CHUN, H.H. (2009) Some practical design aspects of appendages for passenger vessels. *International Journal of Naval Architecture and Ocean Engineering* 1(1), pp. 50–56.
11. JENSEN, N. & LATORRE, R. (1992) Prediction of influence of stern wedges on power boat performance. *Ocean Engineering* 19(3), pp. 303–312.

12. KARAFIATH, G. & FISHER, S.C. (1978) The Effect of Stern Wedges on the Powering Performance. *Naval Engineer Journal* 99, pp. 27–38.
13. KARAFIATH, G., CUSANELLI, D. & LIN, C.W. (1999) Stern wedges and stern flaps for improved powering – US Navy experience. *SNAME Transactions* 107, pp. 67–99.
14. LAHTIHARJU, E., KARPPINEN, T., HELLEVAARA, M. & AITTA, T. (1991) Resistance and Seakeeping Characteristics of Fast Transom Stern Hulls with Systematically Varied Form. *SNAME Transactions* 99, pp. 85–118.
15. MILLWARD, A. (1976) Effect of wedges on the performance characteristics of two planing hulls. *Journal of Ship Research* 20(4), pp. 224–232.
16. PELÁEZ, G., MARTÍN, E., LAMAS, A.M., ULLOA, A.F. & Prieto, D. (2010) *Preliminary study of a new stern device to improve efficiency in a fishing vessel*. 1st International Symposium on Fishing Vessel Energy Efficiency, E-Fishing, Vigo, Spain.
17. SALAS, M. & TAMPIER, G. (2013) Assessment of appendage effect on forward resistance reduction. *Ship Science & Technology*, 7(13), pp. 37–45.
18. SCOGNAMIGLIO, R. (2017) *Prediction of the propulsion performances of planing stepped hulls: CFD in support of experimental towing tank tests*. Ph.D. Thesis, Department of Industrial Engineering, University of Naples Federico.
19. VEYSI, S.T.G., BAKHTIARI, M., GHASSEMI, H. & GHIASI, M. (2015) Toward numerical modeling of the stepped and non-stepped planing hull. *Journal of the Brazilian Society of Mechanical Science and Engineering* 37(6), 1635–1645.
20. YAAKOB, O., SHAMSUDDIN, S. & KOH, K.K. (2004) Stern flap for resistance reduction of planing hull craft: a case study with a fast crew boat model. *Jurnal Teknologi* 41(A), pp. 43–52, doi: 10.11113/jt.v41.689.

Cite as: Ghassemi, M.A., Ghadimi, P., Sajedi, S.M. (2021) The effect of the stern wedge length and height on the drag and trim of a chine-planing hull. *Scientific Journals of the Maritime University of Szczecin, Zeszyty Naukowe Akademii Morskiej w Szczecinie* 67 (139).